

## Phase diagram of a rapidly rotating two-component Bose gas

E. Ö. Karabulut,<sup>1,2</sup> F. Malet,<sup>3</sup> G. M. Kavoulakis,<sup>4</sup> and S. M. Reimann<sup>1</sup>

<sup>1</sup>*Mathematical Physics, LTH, Lund University, P. O. Box 118, SE-22100 Lund, Sweden*

<sup>2</sup>*Department of Physics, Faculty of Science, Selcuk University, TR-42075, Konya, Turkey*

<sup>3</sup>*Department of Theoretical Chemistry and Amsterdam Center for Multiscale Modeling, FEW, Vrije Universiteit, De Boelelaan 1083, 1081HV Amsterdam, The Netherlands*

<sup>4</sup>*Technological Educational Institute of Crete, P. O. Box 1939, GR-71004, Heraklion, Greece*

(Received 15 January 2013; published 9 April 2013)

We derive analytically the phase diagram of a two-component Bose gas confined in an anharmonic potential, which becomes exact and universal in the limit of weak interactions and small anharmonicity of the trapping potential. The transitions between the different phases, which consist of vortex states of single and multiple quantization, are all continuous because of the addition of the second component.

DOI: [10.1103/PhysRevA.87.043609](https://doi.org/10.1103/PhysRevA.87.043609)

PACS number(s): 67.85.-d, 03.75.Kk, 03.75.Lm, 05.30.Jp

### I. INTRODUCTION

One of the remarkable features of cold atomic gases is their high degree of tunability, allowing for a precise and flexible control over most of the experimental parameters, and paving the way for many different potential applications of these systems. On the experimental side, remarkable progress has been made by, e.g., the realization of confining potentials of various functional forms (see, e.g., [1,2]), or by the creation of mixtures of different atomic species (see, e.g., [3]).

Two-component rotating Bose-Einstein condensates have been investigated thoroughly for the case of harmonic confinement [3]. One of the most interesting phenomena is the presence of so-called “coreless vortices” that occur when only one of the two components carries all the angular momentum and forms a vortex state around the second one, which remains at rest at the vortex core [3]. Indeed, the presence of the second, nonrotating component gives rise to an effective anharmonic potential acting on the rotating component, and therefore allows the formation of multiply quantized vortex states [4,5]. These multiply quantized vortex states are not energetically favorable in a single-component system in the case of harmonic confinement.

The rotational properties of a single-component Bose-Einstein condensate in the presence of an anharmonic potential have been addressed previously, employing the Gross-Pitaevskii mean-field approach, or the method of exact diagonalization [6–17]. In the case of harmonic confinement the rotational frequency of the trap  $\Omega$  is limited by the trap frequency  $\omega$  because of the centrifugal force: as  $\Omega \rightarrow \omega$  the system enters a highly correlated regime [18–20], while for  $\Omega > \omega$  the system is not bounded. On the other hand, in the case of anharmonic confinement the system is bounded for any value of  $\Omega$ .

In this study we consider a mixture of two Bose-Einstein condensates, which are confined in an anharmonic potential [21,22]. We investigate the rotational properties of this system as a function of the rotational frequency of the trap and the coupling between the atoms. As we show, in the limit of weak interactions and small anharmonicity of the confining potential one can derive the corresponding phase diagram analytically by solving a quadratic algebraic equation.

Remarkably the phase diagram is exact and universal in these limits.

Our paper is organized as follows. We first focus on the case of zero and sufficiently weak interatomic interactions, where the order parameters of the two species are multiply quantized vortex states. The simplicity of these states then allows us to investigate their stability as the coupling constant between the atoms increases, deriving the phase diagram of the system as a function of the interaction strength and of the rotational frequency of the trap. We finally analyze and interpret our results physically and compare them with those of a single-component system, as the inclusion of a second component changes the corresponding phase diagram rather drastically.

### II. MODEL

We consider a mixture of two distinguishable bosonic atoms, labeled  $A$  and  $B$  with equal mass  $M$ , but with different numbers of atoms  $N_A$  and  $N_B$ . The system is confined in a two-dimensional anharmonic potential of the form

$$V(\rho) = \frac{1}{2}M\omega^2\rho^2\left[1 + \lambda\left(\frac{\rho}{a_0}\right)^2\right], \quad (1)$$

where  $\rho$  is the radial coordinate in cylindrical coordinates,  $\omega$  is the trap frequency,  $a_0 = \sqrt{\hbar/(M\omega)}$  is the oscillator length, and  $\lambda$  is a positive dimensionless parameter measuring the strength of the anharmonicity of the trapping potential. Along the axial direction, the density is assumed to be homogeneous within a width  $Z$ , with a total density per unit length  $\sigma = (N_A + N_B)/Z$ . The intra- and interspecies interactions are modeled as hard-core potentials with scattering lengths for elastic atom-atom collisions  $a_{AA}$ ,  $a_{BB}$ , and  $a_{AB}$ , which are assumed to be repulsive. The general formalism is given for any value of the scattering lengths, while the final results are presented for equal scattering lengths  $a_{AA} = a_{BB} = a_{AB} = a$ . The dimensionless parameter  $\sigma a$  thus gives the “strength” of the interatomic coupling.

Within the mean-field approximation the two order parameters  $\Psi_A$  and  $\Psi_B$  obey coupled, nonlinear, Gross-Pitaevskii-like, differential equations, which in the rotating frame have the

form

$$\begin{aligned} & -\frac{\hbar^2 \nabla^2}{2M} \Psi_i + V(\rho) \Psi_i + (g_{ii} |\Psi_i|^2 + g_{ij} |\Psi_j|^2) \Psi_i \\ & - \Omega \hat{L}_z \Psi_i = \mu_i \Psi_i, \end{aligned} \quad (2)$$

with  $i = A, B$ ;  $j = B, A$ . Here  $\hat{L}_z$  is the axial component of the angular momentum operator,  $\mu_i$  is the chemical potential of each component, and  $g_{ij} = 4\pi \hbar^2 \sigma a_{ij}/M$ .

### III. DISCONTINUOUS TRANSITIONS

Starting with the case of zero coupling,  $\sigma a = 0$ , and small anharmonicity,  $\lambda \ll 1$ , the order parameters  $\Psi_A$  and  $\Psi_B$  are given by the eigenstates of the harmonic potential with no radial nodes,  $\Phi_m(\rho, \phi) \propto \rho^m e^{im\phi} e^{-\rho^2/2a_0^2}$ , where  $m$  is the quantum number that corresponds to the angular momentum  $m\hbar$  (assumed to be positive). The single-particle energy spectrum  $E_m$  of the above states  $\Phi_m$  scales quadratically with  $m$ ,  $E_m = \hbar\omega[1 + m + \lambda(m+1)(m+2)/2]$ , as opposed to the harmonic potential, where  $E_m \propto m$ . As a result, as  $\Omega$  increases, the system undergoes discontinuous phase transitions between the states  $\Phi_m$ .

For weak coupling,  $\sigma a \ll 1$ , one may treat the effect of interactions perturbatively, still neglecting the states with radial nodes. The energy of the system in a state of  $(m, n)$ , where component  $A$  is in the state  $\Phi_m$  and component  $B$  is in the state  $\Phi_n$ , is

$$\begin{aligned} \mathcal{E}_{m,n} = & x_A E_m + x_B E_n + \hbar\omega\sigma a \left( \alpha_{AA} x_A^2 \frac{(2m)!}{2^{2m}(m!)^2} \right. \\ & \left. + \alpha_{BB} x_B^2 \frac{(2n)!}{2^{2n}(n!)^2} + 2\alpha_{AB} x_A x_B \frac{(m+n)!}{2^{m+n}(m!n!)} \right). \end{aligned} \quad (3)$$

Here,  $x_{A,B} = N_{A,B}/N$  and  $\alpha_{ij} = a_{ij}/a$ . The critical frequencies for transitions between different states of  $(m, n)$  can be calculated by comparing the energies in the rotating frame. Figure 1 shows the corresponding phase boundaries for a

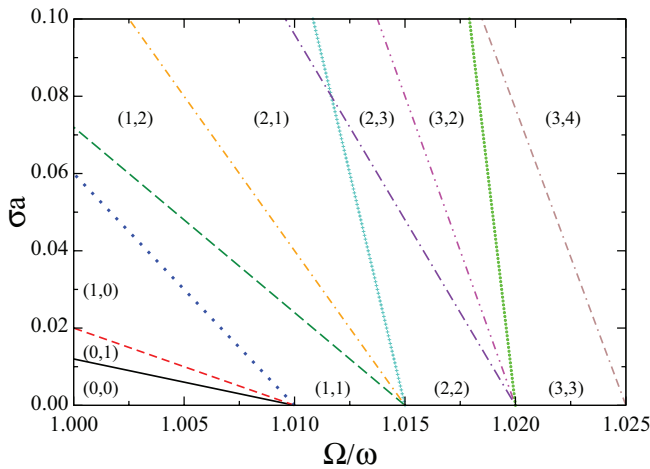


FIG. 1. (Color online) Phase diagram, where the  $x$  axis is the frequency of rotation of the trap  $\Omega/\omega$  and the  $y$  axis is the coupling  $\sigma a$ , for equal scattering lengths. The lines show the discontinuous transitions between the states  $(m, n) \equiv (\Psi_A = \Phi_m; \Psi_B = \Phi_n)$ . Here  $\lambda = 0.005$  and  $N_A/N_B = 2$ .

fixed population imbalance  $N_A/N_B = 2$  and a weak anharmonicity, with  $\lambda = 0.005$ . In the absence of interactions the corresponding critical frequencies are degenerate. However, these degeneracies are lifted by the interactions, as seen in Fig. 1. For a fixed coupling and increasing  $\Omega$  the system first undergoes a (discontinuous) transition from the state  $(0, 0)$  to the state  $(0, 1)$ , where the component with the smaller number of atoms carries all the angular momentum and the other component remains static, a so-called coreless vortex state. Then, with increasing  $\Omega$ , a vortex state forms in the larger component, while the smaller one becomes static, the state  $(1, 0)$ . For an even larger value of  $\Omega$ , there is a transition to the state  $(1, 1)$ , where a vortex state forms in both components. It is interesting that the same result is obtained in the case of mixtures in a purely harmonic potential [4,5].

### IV. CONTINUOUS TRANSITIONS

As the interaction strength increases, the states of multiple quantization become unstable, as the energy of the system is minimized by mixing states of different angular momentum in the order parameters  $\Psi_A$  and  $\Psi_B$ . The multiply quantized vortex states undergo continuous second-order phase transitions. It turns out that the order parameters above the phase boundaries are of the form

$$\Psi_A = c_m \Phi_m + c_{m+q} \Phi_{m+q}, \quad \Psi_B = d_n \Phi_n + d_{n+q} \Phi_{n+q}. \quad (4)$$

Sufficiently close to the phase boundary, the coefficients  $c_m$  and  $d_n$  are of order unity, while the other two coefficients in Eq. (4) tend to zero. For this reason we keep in the energy only the terms which are up to quadratic in  $c_{m+q}$  and  $d_{n+q}$ ,

$$\begin{aligned} \mathcal{E} = & \frac{x_A}{S_A} (E_m c_m^2 + E_{m+q} c_{m+q}^2) + \frac{x_B}{S_B} (E_n d_n^2 + E_{n+q} d_{n+q}^2) \\ & + \frac{x_A^2}{S_A^2} (c_m^4 V_{m,m,m,m}^{AA} + 4c_m^2 c_{m+q}^2 V_{m,m+q,m,m+q}^{AA}) \\ & + \frac{x_B^2}{S_B^2} (d_n^4 V_{n,n,n,n}^{BB} + 4d_n^2 d_{n+q}^2 V_{n,n+q,n,n+q}^{BB}) \\ & + 2 \frac{x_A x_B}{S_A S_B} (c_m^2 d_n^2 V_{m,n,m,n}^{AB} + c_{m+q}^2 d_{n+q}^2 V_{m+q,n,m+q,n}^{AB} \\ & + d_{n+q}^2 c_m^2 V_{m,n+q,m,n+q}^{AB} + 2c_{m+q} d_{n+q} c_m d_n V_{n,m+q,n+q,m}^{AB}), \end{aligned} \quad (5)$$

where  $S_A = c_m^2 + c_{m+q}^2$  and  $S_B = d_n^2 + d_{n+q}^2$ . Since the “pure” states  $\Psi_A = \Phi_m$  and  $\Psi_B = \Phi_n$  provide extrema of the energy in the rotating frame,  $\mathcal{E}_{\text{rot}} = \mathcal{E} - (m+n)\hbar\Omega$ , with respect to  $c_{m+q}$  and  $d_{n+q}$  vanish at the phase boundary. Therefore, the stability of the states of multiple quantization is determined by the eigenvalues of a  $2 \times 2$  matrix whose elements consist of the second-order derivatives of the energy with respect to  $c_{m+q}$  and  $d_{n+q}$ , i.e.,  $M_{1,1} = \partial^2 \mathcal{E}_{\text{rot}} / \partial c_{m+q}^2$ ,  $M_{2,2} = \partial^2 \mathcal{E}_{\text{rot}} / \partial d_{n+q}^2$ , and  $M_{1,2} = \partial^2 \mathcal{E}_{\text{rot}} / \partial c_{m+q} \partial d_{n+q}$ . The resulting matrix elements along the diagonal are

$$\begin{aligned} M_{1,1} = & 2x_A (E_{m+q} - E_m - q\hbar\Omega) + 4x_A^2 [2V_{m,m+q,m,m+q}^{AA} \\ & - V_{m,m,m,m}^{AA}] + 4x_A x_B [V_{m+q,n,m+q,n}^{AB} - V_{m,n,m,n}^{AB}], \end{aligned} \quad (6)$$

$$M_{2,2} = 2x_B(E_{n+q} - E_n - q\hbar\Omega) + 4x_B^2[2V_{n,n+q,n,n+q}^{BB} - V_{n,n,n,n}^{BB}] + 4x_Ax_B[V_{m,n+q,m,n+q}^{AB} - V_{m,n,m,n}^{AB}], \quad (7)$$

while the off-diagonal element is  $M_{1,2} = 4x_Ax_B V_{m,n+q,m+q,n}^{AB}$ , where  $V_{k,l,m,n}^{ij} = \sigma a_{ij} \tilde{V}_{k,l,m,n}$ , with

$$\tilde{V}_{k,l,m,n} = \hbar\omega \frac{(k+l)!}{2^{k+l} \sqrt{k!l!m!n!}} \delta_{k+l,m+n}. \quad (8)$$

When all the eigenvalues of this matrix are positive, the system is stable. However, as soon as any of the eigenvalues becomes negative, an instability occurs via a second-order and continuous phase transition. Assuming equal scattering lengths, we derive the general expression for the phase boundaries of the pure states  $\Psi_A = \Phi_m$  and  $\Psi_B = \Phi_n$  for  $n = m$ , which is given by

$$(\sigma a)_q = \frac{1}{2} \frac{E_{m+q} - E_m - q\hbar\Omega}{\tilde{V}_{m,m,m,m} - \tilde{V}_{m,m+q,m,m+q}}. \quad (9)$$

The parameter  $q$  in the above expression can take any value, provided that  $m + q \geq 0$ .

The result of the calculation described above is shown in the phase diagram depicted in Fig. 2, which is the main result of this study. The phase boundaries corresponding to these continuous transitions (triangular regions) remain in between the straight lines of discontinuous phase transitions of absolute energetic stability shown in Fig. 1, which implies that the transitions between the phases of multiply quantized vortex states are no longer discontinuous. As long as the interaction strength has a nonzero value, they are continuous. The resulting phase diagram obtained for the two-component case in this respect is different from that of the one-component case for which the transitions between phases are found to be both continuous and discontinuous [13].

The part of the phase boundary which represents the instability towards the ‘‘mixed’’ states [i.e., states of the form of Eq. (4)] with  $q = -1$  are vertical due to the fact that

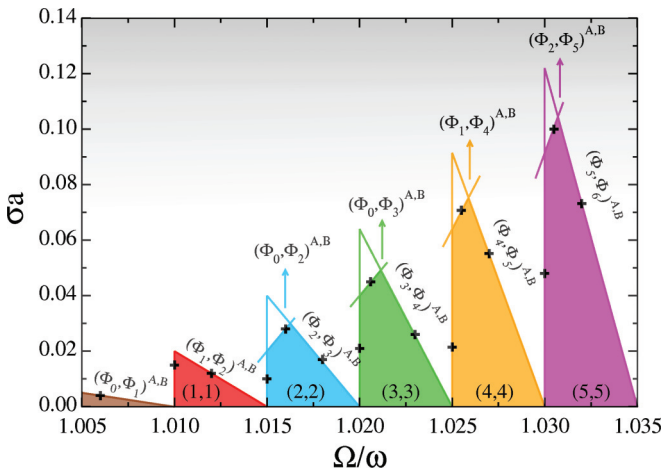


FIG. 2. (Color online) Phase diagram, where the  $x$  axis is the frequency of rotation of the trap  $\Omega/\omega$  and the  $y$  axis is the coupling  $\sigma a$ , for equal scattering lengths. All the lines show continuous transitions. Here  $(m, m) \equiv (\Psi_A = \Phi_m; \Psi_B = \Phi_m)$ , while  $(\Phi_m, \Phi_n)^{A,B} \equiv (\Psi_A = c_m \Phi_m + c_n \Phi_n; \Psi_B = d_m \Phi_m + d_n \Phi_n)$  denotes the states of the form of Eq. (4). Here  $\lambda = 0.005$  and  $N_A/N_B = 2$ .

the denominator of Eq. (9) becomes zero (i.e.,  $\tilde{V}_{m,m,m,m} = \tilde{V}_{m,m-1,m,m-1}$ ) for this unstable mode. The lines corresponding to the unstable mode with  $q = 1$  have negative slope, since

$$(\sigma a)_{q=1} = \hbar\omega \frac{m+1}{\tilde{V}_{m,m,m,m}} [1 - \Omega/\omega + \lambda(m+2)]. \quad (10)$$

Thus, the region of stability takes the shape of a triangle for the pure state with  $m = 1$ . The lines with positive slope cutting the other triangular regions in Fig. 2 denote the phase boundaries of the most unstable mode for the states with  $m \geq 2$ . Accordingly, when  $m = 2$  and  $m \geq 6$ , we find that the most unstable mode corresponds to  $q = -2$ , while for  $m = 3, 4$ , and  $5$ , it turns out that  $q = -3$ .

As the rotational frequency increases, we observe that the region of stability of the multiply quantized vortex states extends further, up to the points where the lines with positive slope cut the triangular regions. For sufficiently large values of  $m$ , demanding that  $(\sigma a)_{q=1} = (\sigma a)_{q=-2}$  and ignoring terms of order of  $1/m$ , we find that  $\Omega/\omega \approx 1 + \lambda(m+1)$ . In other words, for large  $m$ , the lines with positive slope cut the ones with negative slope right at the top of the triangle.

In the phase diagram obtained, we have determined triple points where three phases coexist [10,13]. As seen from Fig. 2, the states (2,2), (3,3), and (4,4) have such triple points, where the two phase boundaries with positive and negative slopes intersect. For example, in the phase (2,2) around the point where the two corresponding phase boundaries cut each other, there is a doubly quantized vortex state, a doubly quantized vortex state with a single vortex around it, and two singly quantized vortex states. To see this, we recall that the states  $\Phi_m(\rho, \phi) \propto z^m$ , where  $z = \rho e^{i\phi}$ . Therefore, if, for example,  $\Psi = c_m \Phi_m + c_{m+q} \Phi_{m+q}$ , then  $\Psi \propto z^m (c_m + c_{m+q} z^q)$ . Since each term  $z - z_0$ , where  $z_0$  is a constant, represents a singly quantized vortex state located at the point  $z_0$  on the  $x$ - $y$  plane, the state  $\Psi$  represents a multiply quantized vortex state of winding number  $m$  that is located at the trap center, plus  $q$  singly quantized vortex states around it [23].

In the fast-rotating regime  $\Omega > \omega$ , the effective potential due to the confinement and the centrifugal potential has a ‘‘Mexican hat’’ form, which leads to a hole in the density of the cloud at the trap center. This hole appears first at the instability of the phase (4,4), which is towards  $(\Phi_1, \Phi_4)$ , as seen in Fig. 3. In this figure we show schematic plots of the density and of the phase of the two order parameters  $\Psi_A$  and  $\Psi_B$  for the

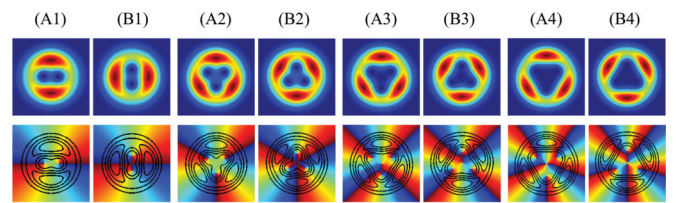


FIG. 3. (Color online) Density (upper plots) and phase (lower plots) of the order parameters of the two components, corresponding to the mixed phases with (A1,B1),  $(\Phi_0, \Phi_2)^{A,B}$ ; (A2,B2):  $(\Phi_0, \Phi_3)^{A,B}$ ; (A3,B3),  $(\Phi_1, \Phi_4)^{A,B}$ ; (A4,B4),  $(\Phi_2, \Phi_5)^{A,B}$  (here  $A_i, B_i$  refer to the two components  $A$  and  $B$ , respectively). The spatial extent of the plots is between  $-6.4a_0$  and  $6.4a_0$  in both directions.

regions above the phases (2,2), (3,3), (4,4), and (5,5). The instability of the phase (3,3) is towards  $(\Phi_0, \Phi_3)$ , which has a nonvanishing density at the center of the cloud. Therefore, up to the phase (3,3) there is no node in the density of the cloud at the center of the trap, while for the phase (4,4) and beyond there is always a hole. From the plots in Fig. 3 we also see that the density minima of the one component coincide with the density maxima of the other component. The total density of the cloud thus remains as close as possible to axial symmetry along these phase boundaries.

The phase diagram that we have evaluated is exact and universal in the limit of weak interactions and weak anharmonicity of the trapping potential. In the single-component case the phase diagram is also universal; however, it is only partly exact [13] because there are also discontinuous phase transitions, where the phase boundaries can be evaluated only approximately. On the other hand, in the present problem all the phase boundaries shown in Fig. 2 are continuous and thus are all exact. The phase diagram is universal in the sense that it is invariant under changes of the degree of anharmonicity  $\lambda$  of the trapping potential (provided that  $\lambda \ll 1$ ), under proper rescaling of the two axes.

## V. NUMERICAL RESULTS

We have confirmed the phase boundaries shown in Fig. 2 numerically for various values of the coupling and of the rotational frequency. Since the transitions are continuous, we start from the phases of multiple quantization found in Fig. 1 for a fixed  $\Omega$  and increasing  $\sigma a$  (or for a fixed  $\sigma a$  and increasing  $\Omega$ ). We choose the initial state  $\Psi_A = \Phi_m$ ,  $\Psi_B = \Phi_n$ , adding some more states with different angular momenta with very small amplitudes, and then propagate those in imaginary time using a fourth-order split-step Fourier method [24].

In the regions of the phase diagram where the multiply quantized vortex states are energetically favorable, the amplitudes of the extra components decay in time. This behavior is seen in the shaded parts of the triangular regions in Fig. 2. On the other hand, outside these regions (but sufficiently close to them) one of the small amplitudes exhibits a steady increase in time, indicating that the multiply quantized vortex states undergo a continuous second-order phase transition, corresponding to the formation of a mixed state of the form of Eq. (4). The clear difference in the temporal imaginary-time evolution of these small amplitudes thus allows us to characterize each point in the phase diagram and also to locate the phase boundaries rather easily. The result of this calculation is shown by the crosses in the phase diagram of Fig. 2. These numerical results are in good agreement with the exact analytic solution. However, the discrepancy between the analytic and the numerical results grows rapidly with increasing  $\lambda$ , since our analytic approach is perturbative.

We stress that the method adopted here makes it possible to verify the location of the phase boundaries, without actually having to evaluate the ground state for the relevant point in the phase diagram, which is a much more demanding calculation, since convergence to the actual lowest-energy state is slow.

## VI. SUMMARY

In summary, we have examined the phase diagram of a mixture of two Bose-Einstein condensed gases confined in an anharmonic potential under rotation, as a function of the strength of the coupling constant and of the rotational frequency of the trap. We have shown that it is possible to derive the corresponding phase diagram analytically, reducing the problem to the evaluation of the roots of an algebraic equation of second degree, which is obtained from the requirement that the determinant of the  $2 \times 2$  matrix defined above vanishes.

It is also remarkable that the presence of a second component makes the solution of this problem in a sense simpler than for its one-component counterpart. In both cases for sufficiently weak interactions the angular momentum is carried by states of multiple quantization. On the other hand, the instability that is caused by the interaction is different in the two cases. In a single-component system a multiply quantized vortex state  $\Psi = \Phi_m$  becomes unstable against a state of the form  $\Psi = c_{m-q}\Phi_{m-q} + c_m\Phi_m + c_{m+q}\Phi_{m+q}$  [13,14]. In the present problem the instability is against states of the form of Eq. (4). Furthermore, in the case of a single component, for sufficiently weak interactions the cloud undergoes discontinuous phase transitions between phases of multiple quantization [13,14]. Here, while there are still phases of vortex states of multiple quantization, the transition between them takes place via continuous transitions. This becomes possible via vortex states which enter the two components successively from infinity, moving continuously towards the trap center.

The phase diagram we have evaluated is exact for sufficiently weak interactions and for small anharmonicity of the trapping potential. As long as these two assumptions are not violated, it is also universal. Furthermore, the phase diagram is independent of the population imbalance; however, this result is valid only under the assumption of equal scattering lengths, provided that both components have a comparable number of atoms, i.e., neither  $N_A$  nor  $N_B \rightarrow 0$ , as otherwise the problem reduces to the case of a single component. In the results of our study we have assumed equal scattering lengths for inter- and intraspecies collisions. In the more general case, i.e., when they are not equal to each other, the phase boundaries are no longer straight lines and they are also dependent on the population imbalance; however, the problem is still of the same level of difficulty. Similar conclusions also hold for the case of unequal masses of the two species.

Last but not least, we should stress that the derived phase diagram is generic for any trapping potential  $V(\rho)$  that rises more rapidly than quadratically. The method adopted here allows one to evaluate the corresponding phase diagram for any such trapping potential. Given the simple and systematic behavior of the evaluated phase diagram, it would be interesting to confirm these results experimentally.

## ACKNOWLEDGMENTS

We acknowledge discussions with A. D. Jackson. This work was financed by the Swedish Research Council and the Nanometer Structure Consortium at Lund University and originated from a collaboration within the ‘‘POLATOM’’ Research

Networking Program of the European Science Foundation (ESF). E.Ö.K. is supported by the Turkish Council of Higher

Education (YÖK) within the scope of the “Post-Doctoral Research Scholarship Program.”

- 
- [1] K. Henderson, C. Ryu, C. MacCormick, and M. G. Boshier, *New J. Phys.* **11**, 043030 (2009).
- [2] Vincent Bretin, Sabine Stock, Yannick Seurin, and Jean Dalibard, *Phys. Rev. Lett.* **92**, 050403 (2004).
- [3] K. Kasamatsu, M. Tsubota, and M. Ueda, *Int. J. Mod. Phys. B* **19**, 1835 (2005).
- [4] S. Bargi, J. Christensson, G. M. Kavoulakis, and S. M. Reimann, *Phys. Rev. Lett.* **98**, 130403 (2007).
- [5] J. Christensson, S. Bargi, K. Kärkkäinen, Y. Yu, G. M. Kavoulakis, M. Manninen, and S. M. Reimann, *New J. Phys.* **10**, 033029 (2008).
- [6] A. L. Fetter, *Phys. Rev. A* **64**, 063608 (2001).
- [7] E. Lundh, *Phys. Rev. A* **65**, 043604 (2002).
- [8] K. Kasamatsu, M. Tsubota, and M. Ueda, *Phys. Rev. A* **66**, 053606 (2002).
- [9] U. R. Fischer and G. Baym, *Phys. Rev. Lett.* **90**, 140402 (2003).
- [10] G. M. Kavoulakis and G. Baym, *New J. Phys.* **5**, 51 (2003).
- [11] E. Lundh, A. Collin, and K.-A. Suominen, *Phys. Rev. Lett.* **92**, 070401 (2004).
- [12] A. Aftalion and I. Danaïla, *Phys. Rev. A* **69**, 033608 (2004).
- [13] A. D. Jackson, G. M. Kavoulakis, and E. Lundh, *Phys. Rev. A* **69**, 053619 (2004).
- [14] A. D. Jackson and G. M. Kavoulakis, *Phys. Rev. A* **70**, 023601 (2004).
- [15] G. M. Kavoulakis, A. D. Jackson, and G. Baym, *Phys. Rev. A* **70**, 043603 (2004).
- [16] S. Bargi, G. M. Kavoulakis, and S. M. Reimann, *Phys. Rev. A* **73**, 033613 (2006).
- [17] M. Correggi, F. Pinsker, N. Rougerie, and J. Yngvason, *Phys. Rev. A* **84**, 053614 (2011).
- [18] N. R. Cooper, *Adv. Phys.* **57**, 539 (2008).
- [19] A. L. Fetter, *Rev. Mod. Phys.* **81**, 647 (2009).
- [20] H. Saarikoski, S. M. Reimann, A. Harju, and M. Manninen, *Rev. Mod. Phys.* **82**, 2785 (2010).
- [21] C.-H. Hsueh, T.-L. Horng, S.-C. Gou, and W. C. Wu, *Phys. Rev. A* **84**, 023610 (2011).
- [22] Pekko Kuopanportti, Jukka A. M. Huhtamäki, and Mikko Möttönen, *Phys. Rev. A* **85**, 043613 (2012).
- [23] G. M. Kavoulakis, B. Mottelson, and C. J. Pethick, *Phys. Rev. A* **62**, 063605 (2000).
- [24] S. A. Chin and E. Krotscheck, *Phys. Rev. E* **72**, 036705 (2005).